

# Sinusoidal Current Source for Bioimpedance Applications Based on a Nonlinear Discrete Time Closed Loop Control Algorithm

Una fuente de corriente sinusoidal para aplicaciones de  
bioimpedancia basado en un algoritmo de control no lineal  
en tiempo discreto

Vladimir Trujillo<sup>a\*</sup>  
Carlos F. Rengifo<sup>b</sup>  
Diego A. Bravo M.<sup>c</sup>

Fecha de Recepción: 18.12.18

Fecha de Aceptación: 08.05.19

DOI: <https://doi.org/10.19053/01217488.v10.n2.2019.8849>

## Abstract

Sinusoidal current sources are fundamental components of electronic equipment used in bioimpedance analysis and in electrical impedance tomography. Currently, these sources are mostly implemented as analog electronic systems. The aim of this paper is to present a new approach to current sources design based on discrete-time closed loop control systems. The experimental results are obtained by implementing the current source in a system of analog and digital programmable blocks, and using as a controller a nonlinear difference equation proposed by the authors. This controller guarantees the convergence of the amplitude of the current flowing through the load, towards a user-desired level. This new control law does not require any parametric adjustment nor knowledge of the load. The developed device is able to produce a sinusoidal current signal of a frequency ranging from 100 Hz to 120 kHz and currents from 500  $\mu$ A to 2 mA. The amplitude error of the current signal remained below 1% for tests performed with resistive-capacitive loads (Cole's type loads). The output impedance is frequency dependent and ranges from 410 k $\Omega$  to 966 k $\Omega$ . The total harmonic distortion is less than 5%. All the proposed system is embedded in the mixed signal device PSOC 5LP, a shunt resistance being the only external component.

**Keywords:** Sinusoidal current sources, bioimpedance, current control loops, nonlinear discrete time control, mixed signal devices..

---

a Departamento de Electrónica, Instrumentación y Control. Universidad del Cauca. Cauca, Calle 5 No. 4-70, Popayán, Colombia.

\*Correo electrónico: vtarias@unicauca.edu.co

b Departamento de Electrónica, Instrumentación y Control. Universidad del Cauca. Cauca, Calle 5 No. 4-70, Popayán, Colombia.

\*Correo electrónico: caferen@unicauca.edu.co

c Departamento de Física. Universidad del Cauca. Cauca, Calle 5 No. 4-70, Popayán, Colombia.

\*Correo electrónico: dibravo@unicauca.edu.co

## Resumen

Las fuentes de corriente sinusoidal son componentes fundamentales de los equipos electrónicos utilizados en el análisis de bioimpedancia y en la tomografía de impedancia eléctrica. Actualmente, estas fuentes se implementan principalmente como sistemas electrónicos analógicos. El objetivo de este documento es presentar un nuevo enfoque para el diseño de fuentes de corriente basado en sistemas de control de lazo cerrado de tiempo discreto. Los resultados experimentales se obtienen implementando la fuente de corriente en un sistema de bloques programables analógicos y digitales, y utilizando como controlador una ecuación de diferencia no lineal propuesta por los autores. Este controlador garantiza la convergencia de la amplitud de la corriente que fluye a través de la carga, hacia un nivel deseado por el usuario. Esta nueva ley de control no requiere ningún ajuste paramétrico ni conocimiento de la carga. El dispositivo desarrollado es capaz de producir una señal de corriente sinusoidal de una frecuencia que van desde 100 Hz a 120 kHz y corrientes desde 500  $\mu$ A hasta 2 mA. El error de amplitud de la señal actual se mantuvo por debajo del 1% para pruebas realizadas con cargas resistivas-capacitivas (tipo Cole). La impedancia de salida es dependiente de la frecuencia y va desde 410 k $\Omega$  hasta 966 k $\Omega$ . La distorsión armónica total es menor al 5%. Todo el sistema propuesto está embebido en dispositivo de señal mixta PSOC 5LP, una resistencia en derivación es el único componente externo.

**Palabras clave:** Fuentes de corriente sinusoidales, bioimpedancia, bucles de control de corriente, no lineales. Control de tiempo discreto, dispositivos de señal mixta..

## 1. INTRODUCTION

Bioimpedance analysis (BIA) is an approach to study the composition of biological tissues [1]. This analysis is generally made by applying a single or multi-frequency current signal to the object under study and then measuring the resulting voltage. Bioimpedance measurements can also be performed by applying a voltage signal and then measuring the resulting current [2], [3]. Bioimpedance has proven to be a very useful, safe and noninvasive technique to detect different types of pathologies such as Alzheimer [4], obesity-associated metabolic derangements [5], malnutrition [6], cancer [7] and to monitor interventions for swelling in minor burns [8]. BIA has been also applied as a principle for development of new medical devices such as the one presented in [9], which was designed to measure the amount of drug released by a transdermal delivery. Another novel device based on BIA is the proposed in [10], which was conceived to detect the arrival of pressure pulse waves in the arteries of the cardiovascular systems. BIA has been also applied to detect intravenous infiltration [11], which is the unintended delivery of fluids into the extravascular space instead of into the vein.

One of the main components of a bioimpedance equipment is the current source which is composed of two main elements: (i) a sinusoidal signal

generator and (ii) a current driver converting a voltage signal into a current. In an ideal case, the transfer function of the second element must be a constant value for all frequencies and any load impedance. To reach this goal, the current driver must have high bandwidth and high output impedance [12]. Nowadays, a great effort is devoted to improve the performance of current drivers.

The trends to design current drivers can be broadly classified into two main groups. The first one and the most widely found is based on the usage of discrete elements like operational amplifiers and feedback networks composed of resistive elements, and in some cases, of a combination of resistors and capacitors, as in [13], [14], [15]. The most well known current drivers are those proposed by Howland [16], [17], [18], [19], [20], Tietze [12] and the current mirror topology [21]. The performance of all these current drivers is limited by two factors: internal capacitances [22] and non-linearities like slew rate, which appear in the operational amplifier at high frequencies. Several works have been devoted to increase both bandwidth and output impedance of the current sources by modifying the feedback network of the operational amplifier or including additional operational amplifiers as in [23], [24], [25]. All of these solutions have in common the increase of analog circuitry with the disadvantages involved in the implementation of electronic systems with

discrete elements. The second trend in current driver design is to implement them in application specific integrated circuits (ASICs). In [26] the authors propose a device based on an operational transconductance amplifier (OTA) implemented in a CMOS integrated circuit. The system includes a negative feedback current loop to overcome the problem of decreasing output impedance as the frequency increases. The current driver presented in [27] is based on the same working principle as [26], but instead of one feedback loop, it uses two of them. Despite of it, the output impedance of [27] is considerably less than that reported in [26]. The architecture presented in [28] is also based on [26], but it solves a problem occurring in all current drivers, which is the phase delay in the output current signal at high frequencies. Other CMOS-based current sources have been proposed as a part of more complex biomedical devices. In [29], the current source is a component of a bioimpedance spectroscopy systems, and in [30] the current source is embedded in an analog front-end for physiological signal recording.

Current sources have been also implemented in Field Programmable Gate Array (FPGA) devices. In [31] the designed device generate a square wave but not a sinusoidal signal as required by bioimpedance studies. In [32] a FPGA based current source is proposed. The current flowing to the load is sensed by using a shunt resistor and the resulting voltage is compared with a reference value, and depending on the result of the comparison, the gain of a programmable amplifier is increased or decreased. However, the authors did not report how such gain is calculated.

Regardless of the approach used, discrete element or ASIC oriented, all current drivers rely on feedback mechanisms to achieve the objective that their transfer function approximates a constant value with zero phase delay for the widest possible range of loads and frequencies. The aforementioned approaches are centered in one component of a current source which is the current driver. Thus, the philosophy of those works does not involve the manipulation of the output of the sinusoidal signal generator. In this paper we propose to manipulate the amplitude of the sinusoidal signal to ensure a current of constant amplitude through the load. This

amplitude is calculated by using a nonlinear discrete time closed loop algorithm which uses as inputs: (i) the desired current amplitude, (ii) the current flowing through the load and (iii) the amplitude of the signal given by the sinusoidal generator in the previous sampling instant.

The current source presented in this paper is fully implemented in a system of configurable analog and digital blocks (PSoC-5LP), not requiring any external element other than a shunt resistor to monitor the current through the load. The first current driver using a programmable device of mixed signal commercially available was implemented in [33]. A novelty aspect of the our system is the use of current digital to analog converters (IDACs) instead of the classical voltage based digital to analog converters (VDACs). The use of IDACs entails two main advantages. First, a bipolar power source for the electronic system is not required, and second, the load is not connected to ground allowing the use tetrapolar electrodes. From a theoretical point of view, the main contribution of the paper is a new control algorithm guaranteeing a constant amplitude sinusoidal current in a load of unknown value.

This paper is composed of seven sections. Section 2 presents current drivers from the perspective of closed loop control systems. Section 3 explains the proposed nonlinear discrete time control algorithm and a mathematical proof of the convergence of the current through the load towards its desired value. Section 4 describes the architecture of the proposed current source. Section 5 presents the experimental results obtained with the implemented prototype. Section 6 contains the discussion of the results and the final section, Section 7, is devoted to the conclusion.

## 2. CURRENT DRIVERS FROM A FEEDBACK CONTROL PERSPECTIVE

Figure 1 shows the classical approach for current source implementation. The voltage  $v_s$ , which is the output of the sinusoidal signal generator, remains unmodified during a current injection experiment and by consequence the performance of the current source relies on the

output impedance and on the bandwidth of the current driver. In the proposed approach, as depicted in Figure 2, the voltage  $v_s$  is modified

by a closed loop controller to produce a current of desired amplitude  $i^d$  in a load of an unknown value.

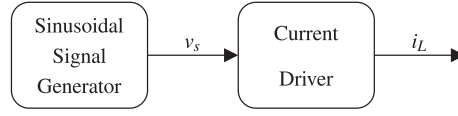


**Figure 1.** Decoupled approach for current sources implementation. The input voltage  $v_s$  to the current driver remains independent of the output  $i_L$  (value of the current in the load).

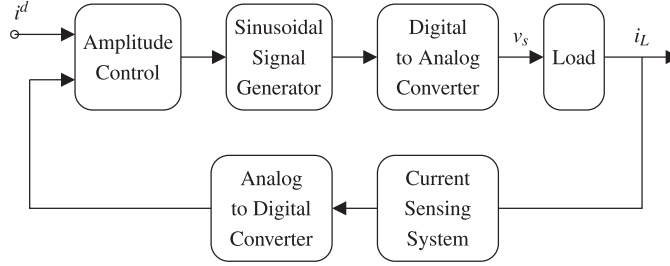


**Figure 2.** Coupled approach for current sources implementation. The input voltage  $v_s$  depends on the current  $i_L$ .

In Figure 2, the current driver can be implemented by using either a discrete element or an ASIC oriented approach. The block named *Amplitude Control* in Figure 2 is any electronic device or a sampled data system guaranteeing the stability of the closed loop system and also the convergence of  $i_L$  towards the desired current  $i^d$ . Based on the closed loop system illustrated in Figure 2, we propose a classification of closed loop control schemes for current sources, depending on the meaning of the variables  $i^d$  and  $i_L$ .

### 2.1 The tracking signal approach

In this approach  $i_L$  is the instantaneous value of the current in the load. The reference  $i^d$  must be a sinusoidal signal indicating the desired value of  $i_L$  at each time instant. The purpose of the block named *Amplitude Control* in Figure 2 is to guarantee the converge of the signal  $i_L(t)$  towards  $i^d(t)$ .

### 2.2 The amplitude control approach

In this approach  $i_L$  is the amplitude of the current in the load. The reference  $i^d$  is the desired value for  $i_L$ . The block *Amplitude Control*, corresponds a sampled data system then the sampling time  $h$  must be equal to the period  $T_o$  of the signal given by the current driver. This is due to the fact that the amplitude of a sinusoidal signal can be changed at most once per period.

As shown in Figure 3, the control  $v_s(kh)$  ( $k = 0, 1, 2, \dots$ ) is the amplitude of the sinusoidal signal applied to the load during the time interval  $[kh, kh + h]$ .

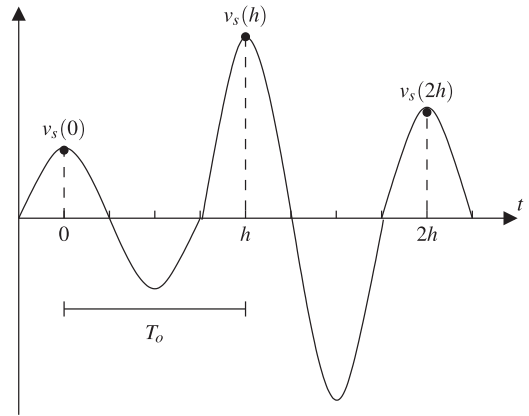


**Figure 3.**  $v_s(kh)$  corresponds to the amplitude of the sinusoidal signal applied to the load during the time interval  $[kh, kh + h]$ .

## 3. THE PROPOSED DISCRETE TIME CURRENT CONTROL ALGORITHM

The current source presented in this paper is based on the amplitude control approach and not in the tracking signal approach because the first one allows to generate signals of higher frequencies than the second one. The proposed control algorithm is described by the following nonlinear difference equation:

$$v_s(kh) = \frac{v_s(kh-h) i^d}{i_L(kh)}, \quad k = 1, 2, \dots \quad (1)$$

The initial value  $v_s(0)$  needs to be greater than zero to avoid the null control signal. Singularities when  $i_L(kh) = 0$  are avoided by limiting the maximal value of  $v_s(kh)$ .  $Z_L(\omega_o)$  represents the total load seen by the current source. That means the contact impedance plus the impedance of the object under study.

**Proposition 1.** *If  $\omega_o$  is the frequency of the sinusoidal signal to be injected to a load impedance with magnitude  $Z_L(\omega_o)$ , then the control described by (1) converges for any  $v_s(0) \neq 0$ , to a value  $v_s^* = i^d Z_L(\omega_o)$  guaranteeing that the steady state amplitude of the current through the load equals to the desired value  $i^d$ .*

*Proof.* If the block *Amplitude Control*, in Figure 2, is defined by equation (1), then the dynamics of the closed loop system is obtained by replacing  $i_L(kh)$  by  $v_s(kh)/Z_L$  in (1)

$$v_s(kh) = \sqrt{i^d Z_L v_s(kh-h)}, \quad k = 1, 2, \dots \quad (2)$$

The solution of (2) can be obtained by induction from  $v_s(h)$ ,  $v_s(2h)$  and  $v_s(3h)$

$$\begin{aligned} v_s(h) &= \left(i^d Z_L\right)^{\left(\frac{1}{2}\right)} v_s(0)^{\frac{1}{2}} \\ v_s(2h) &= \left(i^d Z_L\right)^{\left(\frac{1}{2}+\frac{1}{4}\right)} v_s(0)^{\frac{1}{4}} \\ v_s(3h) &= \left(i^d Z_L\right)^{\left(\frac{1}{2}+\frac{1}{4}+\frac{1}{8}\right)} v_s(0)^{\frac{1}{8}} \\ &\vdots \\ v_s(kh) &= \left(i^d Z_L\right)^{\left(\frac{1}{2}+\frac{1}{4}+\dots+\frac{1}{2^k}\right)} v_s(0)^{\frac{1}{2^k}} \end{aligned} \quad (3)$$

By taking the limit of (3) as  $k$  tends to  $\infty$ , we obtain

$$\lim_{k \rightarrow \infty} v_s(kh) = i^d Z_L \quad (4)$$

The above equation indicates that the control law (1) converges to the voltage  $v_s$  required to obtain a current  $i_L$  equal to  $i^d$ . From the perspective of automatic control point of view, the controller (1) leads to a closed loop system globally asymptotically stable for any  $v_s(0) \neq 0$ .

## 4. ARCHITECTURE OF THE CURRENT SOURCE

In this section we present a current source based on the approach depicted in Figure 2 and implemented in the mixed signal device PSOC 5LP. The non-linear difference equation (1) is implemented as a software component running in the microprocessor of the PSOC system.

### 4.1 Digital to analog current converters

To produce the required sinusoidal voltage signal, the proposed current source uses digital to analog current converters or IDACs instead of the classical voltage based digital to analog converters (VDACs). There are two main reasons for this choice. Firstly, in PSOC 5LP IDACs are faster than VDACs. For the formers the maximal updating frequency is 8 MHz and for the later 1 MHz. Secondly, the output voltage of the VDACs can be configured only in one of two possible ranges, either (i) from 0 to 1,02 volts or from 0 to 4,08 volts. Additionally, by combining an IDAC and a current to voltage converter (I2V) of programmable gain a wider variety of output voltages can be obtained. For example, by fixing the output current of the IDAC to the range 0 to 31,875  $\mu A$  and taking into account that in PSOC 5LP the feedback resistor of the I2Vs must be one of the following values: 20 k $\Omega$ , 30 k $\Omega$ , 40 k $\Omega$ , 80 k $\Omega$ , 120 k $\Omega$ , the number of output voltage ranges increases up to five.

In PSOC 5LP an IDAC can be commuted between source and sink modes in running time, allowing the generation of currents that change direction, as required in bioimpedance studies. Unfortunately, the time required to complete this operation seriously limits the maximal frequency of the sinusoidal signals that can be generated. Our proposal to generate a bipolar voltage signal uses two IDACs and two I2Vs. Figure 4 shows the electrical connection between the two IDACs and two the I2Vs. The two IDACs, denoted as IDAC<sup>+</sup> and IDAC<sup>-</sup>, are configured in source mode. The IDAC<sup>+</sup> generates current only during the positive cycles of the sinusoidal signal. The IDAC<sup>-</sup> generates current only during the negative cycles of the sinusoidal signal. Thus, both IDAC<sup>+</sup> and IDAC<sup>-</sup> generate positive currents defined as follows:

$$\begin{aligned} i_{a^+} &= + \max(0, a_i \sin(\omega_o t)) \\ i_{a^-} &= -\min(0, a_i \sin(\omega_o t)) \end{aligned} \quad (5)$$

In Figure 4 the DC voltage  $v_o$  is defined each time the value of  $R_{fb}$  is changed to guarantee that the input voltage to the buffer amplifiers is non-negative, thus, not requiring bipolar power supplies. The voltages  $v_a$  and  $v_b$  are defined by the following expressions:

$$\begin{aligned} v_a &= v_o - R_{fb} i_{a^-} \\ v_b &= v_o - R_{fb} i_{a^+} \end{aligned}$$

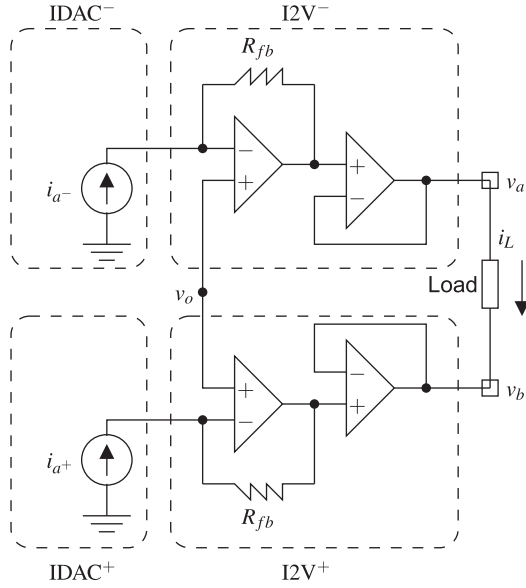


**Figure 4.** Bipolar voltage source composed of two digital to analog current converters (IDACs) and two current to voltage converters (I2Vs).

Figure 5 presents the waveform of the voltages  $v_a$ ,  $v_b$  and  $v_a - v_b$  of the circuit depicted in Figure 4. The difference  $v_a - v_b$  corresponds to a sinusoidal

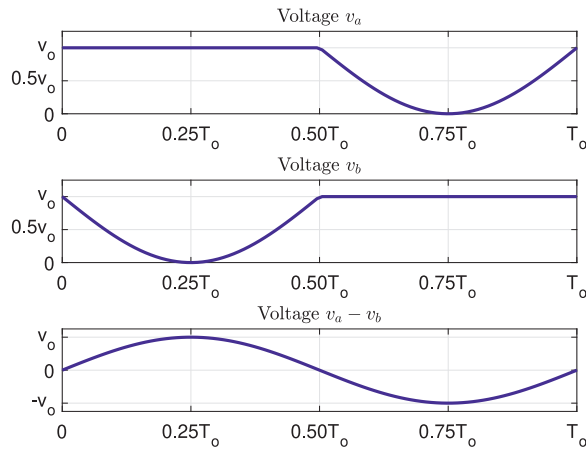


**Figure 5.** Voltages  $v_a$ ,  $v_b$ ,  $v_a - v_b$  in Figure 4. The variable  $T_o$  is the period of the sinusoidal signal.

signal whose amplitude depends on the amplitude of the currents  $i_{a^+}$  and  $i_{a^-}$  and on the value of the feedback resistor  $R_{fb}$ :

$$\begin{aligned} v_a - v_b &= R_{fb} (i_{a^+} - i_{a^-}) \\ &= R_{fb} [\underbrace{\max(0, a_i \sin(\omega_o t))}_{i_{a^+}} - \underbrace{\min(0, a_i \sin(\omega_o t))}_{i_{a^-}}] \\ &= a_i R_{fb} \sin(\omega_o t) \end{aligned}$$

Both IDAC<sup>+</sup> and IDAC<sup>-</sup> have a resolution of 8 bits. Thus, the total resolution of the circuit depicted in Figure 4 is 9 bits.

## 4.2 General block diagram

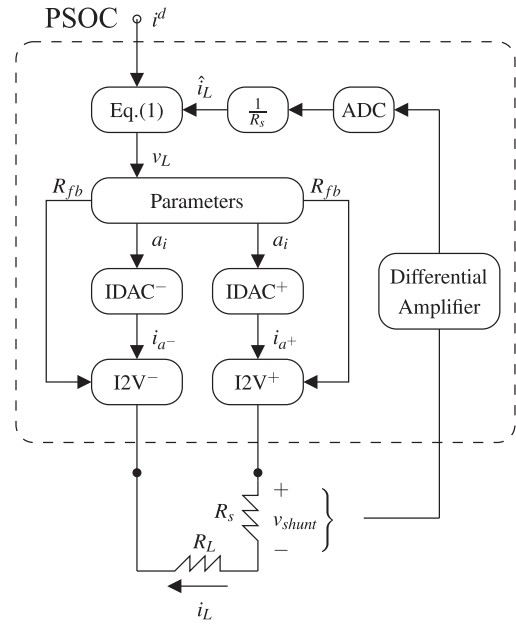


**Figure 6.** Block diagram of the proposed current driver.

A block diagram of the proposed current driver is depicted in Figure 6. The block labeled Eq. (1) contains the algorithm described in the section 3. The variable  $\hat{i}_L$  is an estimation of the amplitude of current flowing to the load, which is calculated from the voltage  $v_{shunt}$  measured in the shunt resistor  $R_s$ . The variable  $v_{shunt}$  is converted by the analog to digital converter block ADC. The block Parameters calculates both, the amplitude  $a_i$  of the sinusoidal currents  $i_{a^+}$  and  $i_{a^-}$  generated by the IDACs and the gain  $R_{fb}$  of the voltage to current converters I2V<sup>+</sup> and I2V<sup>-</sup>. As this current source is based on the amplitude control approach, both Eq.(1) and the block Parameters are executed once for each period of the sinusoidal signal being generated. The values of  $a_i$  and  $R_{fb}$  are calculated by using the following procedure:

1. The value  $v_s(kh)$  given by (1) is used to calculate the value of the  $R_{fb}$  required to obtain  $v_s(kh) = R_{fb} a_{\max}$ , with  $a_{\max} = 31,875 \mu A$  being the maximal current given by the IDACs.
2. As in PSOC 5LP the values of  $R_{fb}$  are restricted to the one of the following values:  $20k\Omega$ ,  $30k\Omega$ ,  $40k\Omega$ ,  $80k\Omega$ ,  $120k\Omega$ , the selected  $R_{fb}$  is the minimal one satisfying  $R_{fb} a_{\max} \geq v_s(kh)$ .
3. The amplitude  $a_i$  is calculated as the quotient between  $v_s(kh)$  and the resistance of  $R_{fb}$  obtained in the step two of this procedure.

## 5. RESULTS

In this section presents the experimental results obtained with the proposed current driver, considering four types of tests: (i) current versus load for a Cole's type load, (ii) current versus frequency for a fixed resistive load, (iii) output impedance and (iv) total harmonic distortion versus load for a fixed frequency. The current through the load is estimated by reading the voltage at the shunt resistor  $R_s = 100 \Omega$  with a digital oscilloscope (*Tektronix TBS 1052B*).

### 5.1 Current versus load resistance for Cole's type load

Figures 8, 9 and 10 present the amplitude of the current as a function of the resistance  $R_\infty$  and the capacitance  $C_1$  of the model depicted in Figure 7. The following frequencies were considered: 1 kHz, 50 kHz and 120 kHz. The value of  $R_1$  is fixed to  $180 \Omega$ . In all the three Figures, the values of the resistance  $R_\infty$  are:  $81 \Omega$ ,  $181 \Omega$ ,  $378 \Omega$ ,  $596 \Omega$ ,  $896 \Omega$ ,  $1000 \Omega$ ,  $1364 \Omega$ ,  $1908 \Omega$ ,  $2350 \Omega$ , and  $2770 \Omega$ .

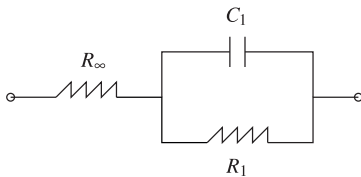


**Figure 7.** Cole's model used as load to test the current source.

### 5.2 Current versus frequency

Figures 11 and 12 present the amplitude of the generated current as a function of the frequency.

The following resistances are used as loads:  $378 \Omega$  and  $3100 \Omega$ , respectively. In both cases, the values of the frequencies are:  $0.1 \text{ kHz}$ ,  $1 \text{ kHz}$ ,  $5 \text{ kHz}$ ,  $10 \text{ kHz}$ ,  $30 \text{ kHz}$ ,  $53 \text{ kHz}$ ,  $80 \text{ kHz}$ ,  $95 \text{ kHz}$  and  $120 \text{ kHz}$ .

### 5.3 Output impedance

Figure 13 presents the Norton's equivalent of the current source. The output impedance is calculated experimentally by using linear regression analysis.

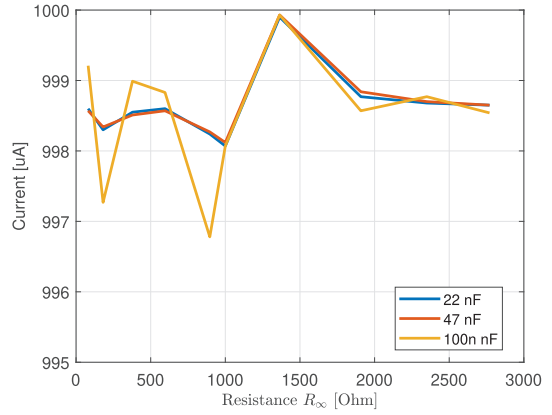


**Figure 8.** Amplitude of the current flowing to the load as a function of the resistance  $R_\infty$  and the capacitance  $C_1$  of a Cole's type load. The frequency is  $1 \text{ kHz}$  and the desired current is  $i^d = 1000 \mu A$ .

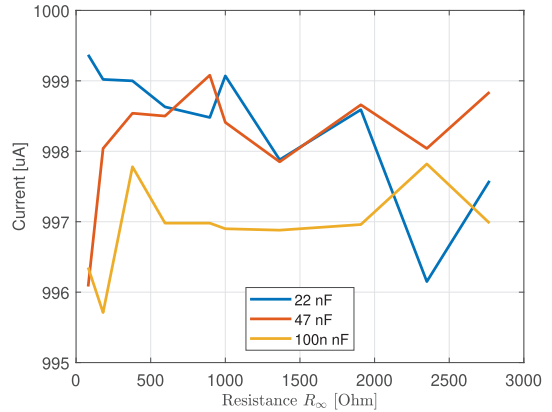


**Figure 9.** Amplitude of the current flowing to the load as a function of the resistance  $R_\infty$  and the capacitance  $C_1$  of a Cole's type load. The frequency is  $50 \text{ kHz}$  and the desired current is  $i^d = 1000 \mu A$ .

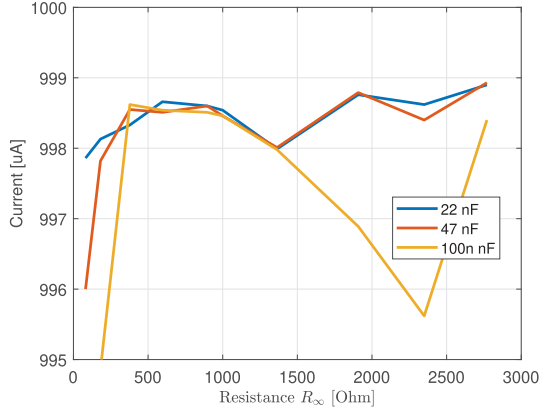


**Figure 10.** Amplitude of the current flowing to the load as a function of the resistance  $R_\infty$  and the capacitance  $C_1$  of a Cole's type load. The frequency is 120 kHz and the desired current is  $i^d = 1000 \mu\text{A}$ .

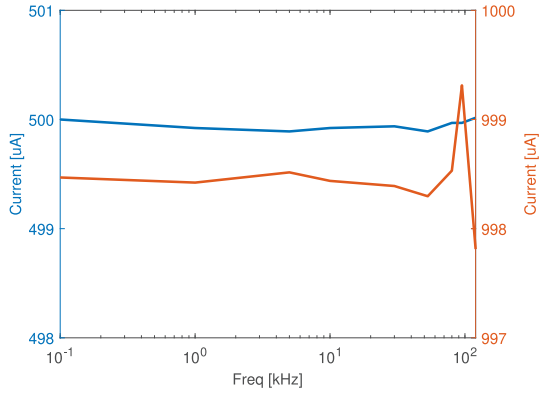


**Figure 11.** Amplitude of the generated current as a function of frequency for a load resistance of  $378 \Omega$ . In color blue the plot for  $i^d = 500 \mu\text{A}$  and the red one for  $i^d = 1000 \mu\text{A}$ .

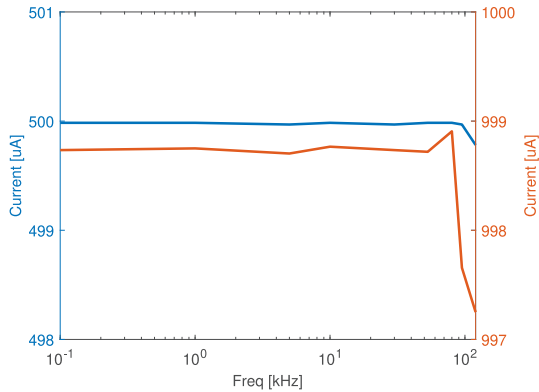


**Figure 12.** Amplitude of the generated current as a function of frequency for a load resistance of  $3100 \Omega$ . In color blue the plot for  $i^d = 500 \mu\text{A}$  and the red one for  $i^d = 1000 \mu\text{A}$ .

The current  $i_L$  through a load  $R_L$  connected to a current source of value  $i^d$  with output impedance  $R_o$ , can be calculated as follows:

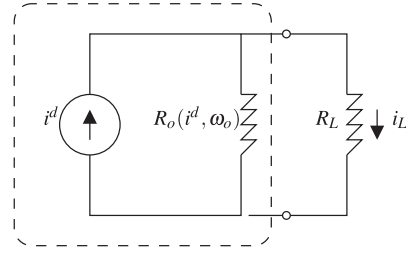


**Figure 13.** Norton's equivalent of the current source.

$$i_L = \frac{R_o}{R_L + R_o} i^d \quad (6)$$

If  $R_L$ ,  $i^d$  and  $i_L$  are known values, then the equation (6) can be easily transformed into the linear equation (7), which relates the current error  $i^d - i_L$  and the measured voltage  $R_L i_L$  through the constant  $R_o$

$$R_L i_L = (i^d - i_L) R_o \quad (7)$$

The linear regression for the data presented in Figure 14 gives the curves presented in Table 1. Figure 14 shows that for the proposed current source the relationship between  $i^d - i_L$  and  $R_L i_L$  is not a straight line and by consequence the output impedance is not constant but dependent on the load  $R_L$  and on the frequency.

**Tabla 1.** Average output impedance as a function of frequency and considering loads ranging from  $378 \Omega$  to  $2770 \Omega$  and  $i^d = 1000 \mu\text{A}$ .

Frequency [kHz]	Average output impedance [kΩ]
0.1	786.73
1.0	711.21
5.0	929.47
10.0	773.51
30.0	839.59
53.0	410.54
80.0	664.37
95.0	655.61
120.0	966.59

#### 5.4 Harmonic distortion versus load resistance

The total harmonic distortion of the current through the load was calculated by using the *Matlab* function *thd*. The samples of the current signal were collected by reading the voltage in the shunt resistor  $R_s$  of Figure 6.

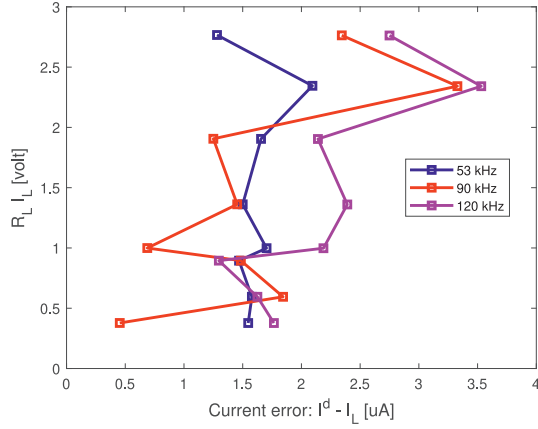


**Figure 14.** Plot relating the current error  $i^d - i_L$  and the measured voltage  $R_L i_L$ . The data does not fit a straight line as expected in a linear current source.

This voltage was measured by using a digital oscilloscope (*Tektronix TBS 1052B*). Figures 15 and 16 present the harmonic distortion as a function of the load resistance for  $i^d = 500 \mu\text{A}$  and  $i^d = 1000 \mu\text{A}$ .

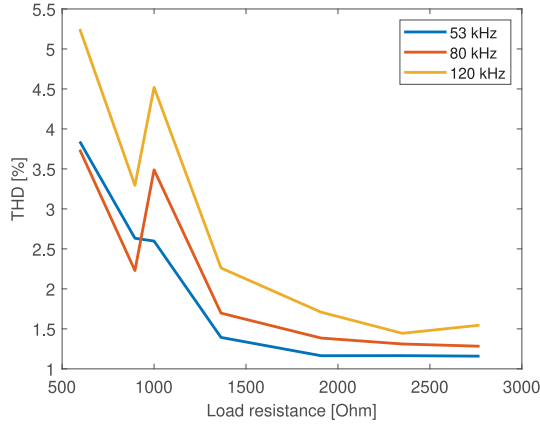


**Figure 15.** Harmonic distortion as a function of the load resistance for  $i^d = 500 \mu\text{A}$ .

## 6. DISCUSSION

The current source presented in this paper uses a feedback control approach to produce a current of desired amplitude and frequency in a load of unknown value. The design combines a software element, which is represented by the nonlinear difference equation (1), and hardware elements like programmable gain amplifiers, IDACs, and one VADC, all of them integrated in a mixed signal chip (see Figure 6). From Figures 8 to 10 it can be seen that the proposed device maintains a constant current through load variations. In Figures 11 and 12 it can be observed that current is almost constant as frequency varies from 100 Hz

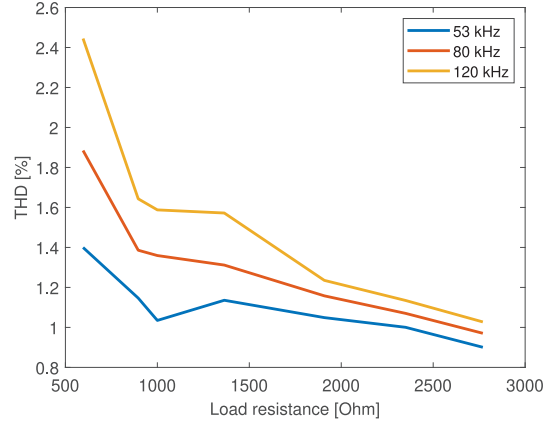


**Figure 16.** Harmonic distortion as a function of the load resistance for  $i^d = 1000 \mu\text{A}$ .

to 120 kHz. These experimental results suggest that the proposed device is a proof of concept for current sources based on the working principle presented in Figure 2.

The maximal frequency generated by the device is limited by the highest frequency of PSOC 5LP IDACs, which is of 8 MHz. By considering 52 samples per period, the maximal frequency of the sinusoidal signal generated is limited to 153,85 kHz ( $8 \text{ MHz}/52$ ). In addition to generating the sinusoidal signal, the PSOC device must recalculate the amplitude of the generated signal by using (1) and to read the analog to digital converter that monitors the current in the load, once per period. All these tasks performed in the same device decrease the maximum frequency up to 120 kHz. However, it is important to clarify that this limitation is not inherent to the approach presented in Figure 2, but to the device used for the implementation.

The output impedance is an aspect of capital importance in current drivers [22], [26], [27], [28] because it guarantees that its gain is not affected by the impedance of the element connected to its output. However, the maximal load is not mainly limited by the output impedance of the current driver but by the output voltage it can produce across the load. For example, in a driver operating a 10 V, the product between the current and the load cannot exceed this value regardless of whether the output impedance is 1 M $\Omega$  or 10 M $\Omega$ . In the proposed device there is no current driver, and a constant amplitude sinusoidal current flowing to a load of unknown value is guaranteed

by the changes in the amplitude of the sinusoidal signal  $v_s$  delivered by the controller (1). As in the case of the current driver approach, in our design the maximal load is also limited by the maximal voltage produced by the circuit of Figure 4, which equals to 4,0625 V. If in Figure 2 the controller ensures the exact convergence of  $i_L$  towards  $i^d$  for a given range of frequencies, currents and loads, then the steady state output impedance of the current source is theoretically infinite for those values. In practice, the convergence of  $i_L$  is limited by the precision with which the voltage  $v_s$  is generated and with which the current  $i_L$  is estimated. For the implementation in PSOC of the control approach of Figure 2, the difference between the desired and the measured currents is caused by the quantization of the two IDACs and of the ADC reading the voltage at the shunt resistor. Another source of error is the limited number of feedback resistors  $R_{fb}$  used in Figure 4. The linear regression for the data presented in Figure 14 shows that for the proposed current source the relationship between  $i^d - i_L$  and  $R_L i_L$  is not a straight line and by consequence the output impedance is not constant but dependent on the load  $R_L$  and on the frequency of the generated signal. This nonlinear behaviour is caused by the three steps computation procedure presented at the end of Section 4.2. For this current source the average output impedance ranges from 410,54 k $\Omega$  to 966,56 k $\Omega$ , which is close to the values obtained by [19], [27] and [34], but below as compared to that reported in [28].

The total amplitude harmonic distortion is greater for low impedance loads (see Figures 15 and 16). This phenomenon is originated by the quantization of the IDACs. Low currents through low impedances require of sinusoidal signals of small amplitude which are generated by using only the least significant bits of the IDAC register. For example, to circulate a current of 500  $\mu$ A through a resistance of 378  $\Omega$  requires a sinusoidal signal with an amplitude of 189 mV. Considering that the lowest value of  $R_{fb}$  is 20 k $\Omega$ , the peak amplitude of the current produced by the IDACs must be 9,45  $\mu$ A, which implies that only the 6 least significant bits are used.

The proposed approach for current sources implementation guarantees that the amplitude of the current through the load is equal to its desired value  $i^d$ . However, the proposed device does not control the phase of the current in the load. The sinusoidal signal  $v_s$  generated by the controller of the Figure 2, always has zero phase angle. It implies that the phase of  $i_L$  remains dependent on the capacitance of the load and on the working frequency  $\omega_o$ . The lack of phase control in our current source does not prevent its usage in BIA, because the phase plot can be obtained from the gain plot, providing that the load is a linear, stable and minimum-phase system. In [35] the authors propose a method to obtain phase information from magnitude measurements based on the Kramers-Kronig transform. Additionally, techniques to extract the parameters of single and double dispersion Cole models from magnitude response measurements have been respectively proposed in [36] and [37]. Furthermore, some BIA rely only on amplitude measures as in [38] and [39].

## CONCLUSION

An alternative working principle for current source design has been proposed. It is based on a discrete time nonlinear algorithm ensuring the convergence of the measured current towards its desired value. The algorithm does not require any parameter tuning. The proposed approach was implemented in a mixed signal device, obtaining low differences between the desired and the measured current for frequencies near to the maximal frequency that the IDACs can operate. Future works will be devoted to enhance the nonlinear algorithm to control both the amplitude and the phase of current in the load. Another aspect that will be addressed is the system used for the implementation of the current source.

## ACKNOWLEDGMENT

The authors would like to recognize and express their sincere gratitude to Universidad del Cauca [501100005682], Colombia (UNICAUCA) for the financial support granted during this project.

## REFERENCIAS

- [1] H. Caytak, A. Boyle, A. Adler, and M. Bolic, "Bioimpedance spectroscopy processing and applications," in *Reference Module in Biomedical Sciences*, Elsevier, 2017.
- [2] D. Bouchaala, Q. Shi, X. Chen, O. Kanoun, and N. Derbel, "Comparative study of voltage controlled current sources for bioimpedance measurements," in *International Multi-Conference on Systems, Signals Devices*, pp. 1–6, March 2012.
- [3] T. Qureshi, C. Chatwin, and W. Wang, "Bioimpedance excitation system: A comparison of voltage source and current source designs," *APCBEE Procedia*, vol. 7, pp. 42 – 47, 2013.
- [4] E. Mereu, V. Succa, R. Buffa, C. Sanna, R. M. Mereu, O. Catte, and E. Marini, "Total body and arm bioimpedance in patients with Alzheimer's disease," *Experimental Gerontology*, vol. 102, pp. 145 – 148, 2018.
- [5] J. Gómez-Ambrosi, I. González-Crespo, V. Catalán, A. Rodríguez, R. Moncada, V. Valentí, S. Romero, B. Ramíez, C. Silva, M. J. Gil, J. Salvador, A. Benito, I. Colina, and G. Frühbeck, "Clinical usefulness of abdominal bioimpedance (viscan) in the determination of visceral fat and its application in the diagnosis and management of obesity and its comorbidities," *Clinical Nutrition*, vol. 37, no. 2, pp. 580 – 589, 2018.
- [6] M. P. R. del Río, M. A. Camina-Martín, L. Moya-Gago, S. de-la Cruz-Marcos, V. Malafarina, and B. de Mateo-Silleras, "Vector bioimpedance detects situations of malnutrition not identified by the indicators commonly used in geriatric nutritional assessment: A pi- lot study," *Experimental Gerontology*, vol. 85, no. Supplement C, pp. 108 – 111, 2016.
- [7] G. S. Sarode, S. C. Sarode, M. Kulkarni, S. Karmarkar, and S. Patil, "Role of bioimpedance in cancer detection: A brief review," *International Journal of Dental Science and Research*, vol. 3, no. 1, pp. 15 – 21, 2016.
- [8] P. Kenworthy, T. L. Grisbrook, M. Phillips, P. Gittings, F. M. Wood, W. Gibson, and D. W. Edgar, "Bioimpedance spectroscopy: A technique to monitor interventions for swelling in minor burns," *Burns*, vol. 43, no. 8, pp. 1725 – 1735, 2017.
- [9] P. Arpaia, U. Cesaro, and N. Moccaldi, "A bioimpedance meter to measure drug in trans-dermal delivery," *IEEE Transactions on Instrumentation and Measurement*, pp. 1 – 8, 2018. Early access.
- [10] R. Kusche, P. Klimach, and M. Ryschka, "A multichannel real-time bioimpedance measurement device for pulse wave analysis," *IEEE Transactions on Biomedical Circuits and Systems*, pp. 1 – 9, 2018. Early access.
- [11] A. O. Bicen, L. L. West, L. Cesar, and O. T. Inan, "Toward non-invasive and automatic intravenous infiltration detection: Evaluation of bioimpedance and skin strain in a pig model," *IEEE Journal of Translational Engineering in Health and Medicine*, pp. 1–1, 2018.
- [12] D. Bouchaala, O. Kanoun, and N. Derbel, "High accurate and wideband current excitation for bioimpedance health monitoring systems," *Measurement*, vol. 79, no. 1, pp. 339 – 348, 2016.
- [13] A. S. Ross, G. J. Saulnier, J. C. Newell, and D. Isaacson, "Current source design for electrical impedance tomography," *Physiological Measurement*, vol. 24, no. 2, 2003.
- [14] A. Tucker, R. Fox, and R. Sadleir, "Biocompatible, high precision, wideband, improved Howland current source with lead-lag compensation," *IEEE Transactions on Biomedical Circuits and Systems*, vol. 7, no. 1, pp. 63 – 70, 2013.

- [15] S. Rossi, M. Pessione, V. Radicioni, G. Baglione, M. Vatteroni, P. Dario, and L. Della Torre, "A low power bioimpedance module for wearable systems," *Sensors and Actuators A: Physical*, vol. 232, pp. 359 – 367, 2015.
- [16] D. H. Sheingold, "Impedance & admittance transformations using operational," *The lightning empiricist*, vol. 12, Jan. 1964.
- [17] M. Rafiei-Naeini and H. McCann, "Low-noise current excitation sub-system for medical EIT," *Physiological Measurement*, vol. 29, no. 6, 2008.
- [18] R. A. Stiz, P. Bertemes, A. Ramos, and V. C. Vincence, "Wide band Howland bipolar current source using AGC amplifier," *IEEE Latin America Transactions*, vol. 7, pp. 514 – 518, Sept 2009.
- [19] Y. Mohamadou, T. I. Oh, H. Wi, H. Sohal, A. Farooq, E. J. Woo, and A. L. McEwan, "Performance evaluation of wideband bioimpedance spectroscopy using constant voltage source and constant current source," *Measurement Science and Technology*, vol. 23, no. 10, 2012.
- [20] A. Mahnam, H. Yazdanian, and M. M. Samani, "Comprehensive study of Howland circuit with non-ideal components to design high performance current pumps," *Measurement*, vol. 82, pp. 94 – 104, 2016.
- [21] P. Bertemes Filho, *Tissue characterisation using an impedance spectroscopy probe*. PhD thesis, University of Sheffield, 2002.
- [22] H. Yazdanian, M. Samani, and A. Mahanm, "Characteristics of the Howland current source for bioelectric impedance measurements systems," in *20th Iranian Conference on Biomedical Engineering (ICBME)*, pp. 189 – 193, Dec 2013.
- [23] P. J. Riu, J. Rosell, A. Lozano, and R. Pallàs-Areny, "A broadband system for multifrequency static imaging in electrical impedance tomography," *Clinical Physics and Physiological Measurement*, vol. 13, no. A, 1992.
- [24] R. Bragos, J. Rosell, and P. Riu, "A wide-band AC-coupled current source for electrical impedance tomography," *Physiological Measurement*, vol. 15, no. 2A, 1994.
- [25] A. Al-Obaidi and M. Meribout, "A new enhanced Howland voltage controlled current source circuit for EIT applications," in *IEEE Conference and Exhibition (GCC)*, pp. 327 – 330, Feb 2011.
- [26] H. Hong, A. Demosthenous, I. F. Triantis, P. Langlois, and R. Bayford, "A high output impedance cmos current driver for bioimpedance measurements," in *2010 Biomedical Circuits and Systems Conference (BioCAS)*, pp. 230 – 233, Nov 2010.
- [27] L. Constantinou, I. F. Triantis, R. Bayford, and A. Demosthenous, "High-power CMOS current driver with accurate transconductance for electrical impedance tomography," *IEEE Transactions on Biomedical Circuits and Systems*, vol. 8, pp. 575 – 583, Aug 2014.
- [28] P. J. Langlois, N. Neshatvar, and A. Demosthenous, "A sinusoidal current driver with an extended frequency range and multifrequency operation for bioimpedance applications," *IEEE Transactions on Biomedical Circuits and Systems*, vol. 9, no. 3, pp. 401 – 411, 2015.
- [29] R. Onet, R. Onet, A. Rusu, and S. Rodriguez, "High-purity and wide-range signal generator for bioimpedance spectroscopy," *IEEE Transactions on Circuits and Systems II: Express Briefs*, pp. 1–1, 2018. Early access.
- [30] J. Xu, M. Konijnenburg, H. Ha, R. van Wegberg, S. Song, D. Blanco-Almazán, C. V. Hoof, and N. V. Helleputte, "A 36 uw 1.1 mm<sup>2</sup> reconfigurable analog front-end for cardiovascular and respiratory signals recording," *IEEE Transactions on Biomedical Circuits and Systems*, pp. 1–10, 2018.

- [31] Z. Hamed, H. Tenhunen, and G. Yang, “A programmable low power current source for bioimpedance measurement: Towards a wearable personalized health assistant,” in *37th Annual International Conference of the IEEE Engineering in Medicine and Biology Society (EMBC)*, pp. 2038 – 2042, Aug 2015.
- [32] N. Li, H. Xu, W. Wang, and W. Zhang, “High-speed digital-controlled variable voltage source with current monitor for EIT application,” in *4th International Conference on Biomedical Engineering and Informatics (BMEI)*, pp. 1110 – 1113, Oct 2011.
- [33] J. J. Cabrera-López, J. Velasco-Medina, E. R. Denis, J. F. B. Calderón, and O. J. G. Guevara, “Bioimpedance measurement using mixed-signal embedded system,” in *2016 IEEE 7th Latin American Symposium on Circuits Systems (LASCAS)*, pp. 335–338, Feb 2016.
- [34] H. Hong, M. Rahal, A. Demosthenous, and R. H. Bayford, “Comparison of a new integrated current source with the modified Howland circuit for EIT applications,” *Physiological Measurement*, vol. 30, no. 10, 2009.
- [35] A. A. Al-Ali, A. S. Elwakil, B. J. Maundy, and T. J. Freeborn, “Extraction of phase information from magnitude-only bioimpedance measurements using a modified Kramers–Kronig transform,” *Circuits, Systems, and Signal Processing*, Dec 2017.
- [36] B. Maundy, A. Elwakil, and A. Allagui, “Extracting the parameters of the single-dispersion Cole bioimpedance model using a magnitude-only method,” *Computers and Electronics in Agriculture*, vol. 119, pp. 153 – 157, 2015.
- [37] T. J. Freeborn, B. Maundy, and A. S. Elwakil, “Extracting the parameters of the double-dispersion Cole bioimpedance model from magnitude response measurements,” *Medical & Biological Engineering & Computing*, vol. 52, no. 9, pp. 749 – 758, 2014.
- [38] J. Ramos, J. Ausín, G. Torelli, and J. Duque-Carrillo, “A wireless bioimpedance device for abdominal fatness monitoring,” *Procedia Chemistry*, vol. 1, no. 1, pp. 1259 – 1262, 2009. Proceedings of the Eurosensors XXIII conference.
- [39] T. J. Freeborn, A. S. Elwakil, and B. Maundy, “Variability of Cole-model bioimpedance parameters using magnitude-only measurements of apples from a two-electrode configuration,” *International Journal of Food Properties*, vol. 20, no. sup1, pp. S507–S519, 2017.